

# Efficient quantum transport in disordered interacting many-body networks

Adrian Ortega,<sup>1,\*</sup> Thomas Stegmann,<sup>1,†</sup> and Luis Benet<sup>1,2,‡</sup>

<sup>1</sup>*Instituto de Ciencias Físicas, Universidad Nacional Autónoma de México, Cuernavaca, México*

<sup>2</sup>*Centro Internacional de Ciencias, Cuernavaca, México*

(Dated: 03 October 2016)

The coherent transport of  $n$  fermions in disordered networks of  $l$  single-particle states connected by  $k$ -body interactions is studied. These networks are modeled by embedded Gaussian random matrix ensemble (EGE). The conductance bandwidth as well as the ensemble-averaged total current attain their maximal values if the system is highly filled  $n \sim l - 1$  and  $k \sim n/2$ . For the cases  $k = 1$  and  $k = n$  the bandwidth is minimal. We show that for all parameters the transport is enhanced significantly whenever centrosymmetric ensemble (csEGE) are considered. In this case the transmission shows numerous resonances of perfect transport. Analyzing the transmission by spectral decomposition, we find that centrosymmetry induces strong correlations and enhances the extrema of the distributions. This suppresses destructive interference effects in the system and thus, causes backscattering-free transmission resonances which enhance the overall transport. The distribution of the total current for the csEGE has a very large dominating peak for  $n = l - 1$ , close to the highest observed currents.

PACS numbers: 05.60.Gg, 73.23.-b, 87.15.-v

## I. INTRODUCTION AND MOTIVATION

The motivation of our study is to understand properties of certain biomolecules such as the Fenna-Mathews-Oslon (FMO) light-harvesting complex [1], as well as the engineering of quantum devices, like quantum buses based on spin chains [2]. These systems display a remarkably efficient transport of electronic excitations or quantum states. In the context of biomolecules for which quantum effects may play a role, it seems realistic that models describing excitonic transport have to display disorder [3–6]. Therefore one way to look at the problem is modeling the system by means of purely stochastic approaches, such as those of random matrix theory (RMT) [7, 8]. Quantum spin chains [9] are candidates for playing the role of quantum buses between quantum processors in a quantum computer. The transfer efficiency of states between the ends of the chain can happen with probability 1, for a very particular interaction [10–13]. There are models for treating the random coupling case such as [14, 15], but they do not address the effects of many-body interactions, which we consider using the embedded random-matrix ensemble [16, 17].

In our previous work [18] we have studied the efficiency of small bosonic and fermionic disordered networks generated by the embedded Gaussian random matrix ensemble (EGE) for closed systems. In this work, we open (in the scattering sense) the fermionic many-body interacting system and analyze the transmission and current averaged over the ensemble. The question which we address is how the coherent transport between two states of a small disordered interacting quantum system can

be improved. We concentrate in small networks since the Hilbert space dimension of FMO molecules and spin chains is rather small [3–6, 11–13]. We will show that the presence of centrosymmetry [19] in the ensemble is again a fundamental building block to enhance transport in disordered quantum networks [5, 6, 10, 11].

We consider a system of  $l$  single-particle states, which are coupled via  $k$ -body interactions and occupied by  $n$  fermions. The Hamiltonian of this system is taken from embedded Gaussian ensemble of random matrices (EGE). The transport between two states of the Hilbert space of this system is calculated by means of the nonequilibrium Green's function (NEGF) method. Details on the model and our method are provided in Section II.

The energy resolved transmission  $T(E)$  for two typical members of the ensemble is shown in Figure 1. In both cases the transmission shows resonances which are located approximately at the eigenenergies of the Hamiltonian. Many resonances of perfect transport ( $T = 1$ ) can be observed if the Hamiltonian is centrosymmetric; see the red curve in Figure 1. Moreover, our objective here is not restricted to certain energies but on improving the transport in the whole conduction band, which is achieved by centrosymmetry.

In Section III, we shall discuss in detail the enhancement of the transport properties due to centrosymmetry as well as its effect on the statistical properties of the system. In particular, we find that important spectral correlations appear for the open centrosymmetric Hamiltonian. These, combined with the structure of the eigenfunctions, yield higher and broader transmission resonances, as well as a wider conduction band, which result in an enhanced current. The conclusions and outlook are presented in Section IV.

\* adrianortega@fis.unam.mx

† stegmann@icf.unam.mx

‡ benet@fis.unam.mx

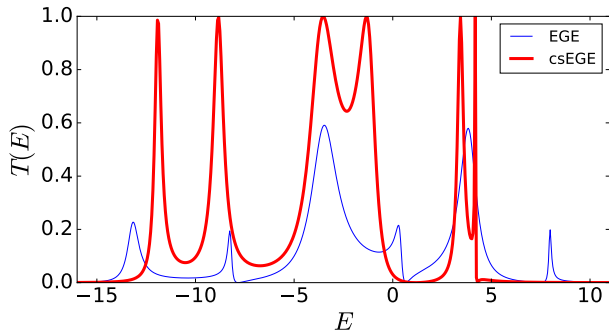


Figure 1. (color online) Transmission  $T(E)$  as a function of the energy  $E$  for two typical members of the random matrix ensemble. The parameters are  $l = 6$ ,  $n = 5$ ,  $k = 3$ . In both cases resonances can be observed which are approximately at the eigenenergies of the Hamiltonian. If the Hamiltonian is centrosymmetric (red-thick curve), we observe numerous resonances of perfect transport ( $T = 1$ ). The transmission increases significantly compared to a Hamiltonian without this symmetry property (blue-thin curve).

## II. MODEL AND METHODS

### A. Embedded random matrix ensemble for disordered interacting systems

We consider a set of  $l$  degenerate (fermionic) single-particle states  $|j\rangle$ , with  $j = 1, 2, \dots, l$ . The associated creation and annihilation operators are  $a_j^\dagger$  and  $a_j$ , with  $j = 1, \dots, l$ . They obey the usual anti-commutation relations which characterize fermions. We define the operators that create a normalized state with  $k < l$  fermions from the vacuum state as  $\psi_{k;\alpha}^\dagger = \psi_{j_1, \dots, j_k}^\dagger = \prod_{s=1}^k a_{j_s}^\dagger$ , with the convention that the indices are ordered increasingly  $j_1 < j_2 < \dots < j_k$ . The index  $\alpha$  in the many-body operators labels the specific occupation given by the  $j_s$ , and simplifies the notation. The corresponding annihilation operator  $\psi_{k;\alpha}$  is constructed analogously.

The random  $k$ -body Hamiltonian reads

$$H_k = \sum_{\alpha, \gamma} v_{k;\alpha, \gamma} \psi_{k;\alpha}^\dagger \psi_{k;\gamma}, \quad (1)$$

which takes into account interactions between up to  $k$  particles. The coefficients  $v_{k;\alpha, \gamma}$  are randomly distributed independent Gaussian variables with zero mean and unit variance

$$\overline{v_{k;\alpha, \gamma} v_{k;\alpha', \gamma'}} = \delta_{\alpha, \alpha'} \delta_{\gamma, \gamma'} + \delta_{\alpha, \alpha'} \delta_{\gamma, \gamma'}. \quad (2)$$

The Hamiltonian  $H_k$  acts on a Hilbert space spanned by distributing  $n \geq k$  particles on the  $l > n$  single-particle states. A complete set of basis states is given by the set  $\psi_{n;\alpha}^\dagger |0\rangle$ . The dimension of the Hilbert space is  $N = \binom{l}{n}$ . This defines the  $k$ -body embedded Gaussian orthogonal ensemble of random matrices for fermions [16, 17].

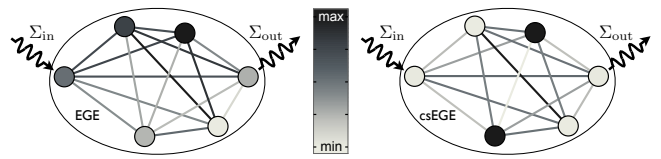


Figure 2. Graph representations of Hamiltonians from the EGE (left) and the csEGE (right). The shading of the nodes and links corresponds to the matrix element  $\langle \nu | V_k | \mu \rangle$ . The transmission between the ingoing and outgoing states, indicated by  $\Sigma_{\text{in/out}}$ , is shown in Figure 1.

By construction, the case  $k = n$  is identical to the canonical ensemble of random matrix theory [8], i.e. to the Gaussian orthogonal ensemble (GOE). For  $k < n$ , the matrix elements of  $H_k$  may be identical to zero and display correlations. Zeros appear whenever no  $k$ -body operator exist that links together the  $n$ -body states. Correlations arise because matrix elements of  $H_k$  not related by symmetry may be identical.

The representation of the Hamiltonian  $H_k$  can be interpreted as a graph, see Figure 2. Each node represents a  $n$ -body many-particle state  $|\mu\rangle = \psi_{n;\mu}^\dagger |0\rangle$ . The number of nodes in the graph is determined by the dimension of the Hilbert space  $N$ . A pair of nodes is linked, if the matrix element  $\langle \nu | V_k | \mu \rangle \neq 0$ . The graphs generated by the fermionic EGE model are regular graphs [20], because each node has the same number of links.

### B. Centrosymmetry in the embedded Gaussian ensemble

Centrosymmetry is an important concept to enhance the efficiency [4, 18] and, as we shall see below, transport. A symmetric  $N \times N$  matrix  $A$  is centrosymmetric if  $[A, J] = 0$ , where  $J_{i,j} \equiv \delta_{i, N-j+1}$  is the *exchange matrix* [19] or, equivalently, an anti-diagonal unit matrix. One can therefore construct a centrosymmetric matrix by imposing that a real symmetric matrix  $A$  commutes with  $J$ .

Imposing centrosymmetry to the  $k$ -body embedded ensemble is subtle. Following [18], it can be introduced either at the one-particle level, which is the core for the definition of the  $k$ - and  $n$ -particle Hilbert spaces, at the  $k$ -body level, where the actual (random) parameters of the embedded ensemble are set, or at the  $n$ -body level, which defines the dynamics. The latter cases can be implemented following the procedure described in Ref. [19] (c.f. Lemmas 2(i) and 2(ii)), though it is not clear whether we should choose the  $k$  body space or the  $n$  body space. Since the one-particle states are the building blocks to construct both the  $k$ -body particle states and the  $n$ -body particle states, we shall define centrosymmetry at the one-particle level. Note that this approach yields a consistent treatment of more realistic situations, e.g. a system that includes a one-body (mean-field) term and a two-body (residual) interaction,  $H = H_{k=1} + H_{k=2}$ .

Considering that centrosymmetry is introduced at the one-particle level, we define it by  $J_1 |j\rangle = |l - j + 1\rangle$  for  $j = 1, 2, \dots, l$ , whose matrix representation in the one-body basis is precisely the exchange matrix. For two fermions, we define  $J_2 \psi_{2;j_1,j_2}^\dagger = J_1 a_{j_1}^\dagger J_1 a_{j_2}^\dagger = -\psi_{2;l-j_2+1,l-j_1+1}^\dagger$ . In the last equation we followed the convention that the indices are arranged in increasing order; then, the fermionic anticommutation relations impose a global minus sign, which can be safely ignored. This is generalized for  $k$  particles as

$$J_k \psi_{k;j_1,\dots,j_k}^\dagger = \prod_{s=1}^k J_1 a_{j_s}^\dagger = \psi_{k;l-j_k+1,\dots,l-j_1+1}^\dagger, \quad (3)$$

where we have dropped any global minus sign. We note that in general the matrix  $J_k$ , as defined by Eq. (3), may not be an exchange matrix. This follows from the possible existence of more than one state that is mapped by  $J_k$  onto itself; in this case, we shall say that  $J_k$  is a *partial* exchange matrix. As an example, considering  $l = 4$  single-particle states and two-body ( $k = 2$ ) interactions, the  $k$ -particle space has dimension 6. In this case,  $J_2 \psi_{2;2,3}^\dagger = \psi_{2;2,3}^\dagger$  and  $J_2 \psi_{2;1,4}^\dagger = \psi_{2;1,4}^\dagger$ , ignoring the minus signs mentioned above, since under  $J_1$  we have  $|1\rangle \rightarrow |4\rangle$  and  $|2\rangle \rightarrow |3\rangle$ . Then, the entries in the  $J_2$  matrix elements for these basis states are 1 in the diagonal and  $J_2$  is a partial exchange matrix. In contrast, for the case  $l = 4$  and  $k = 1, 3$  the resulting matrices  $J_1$  and  $J_3$  are exchange matrices.

### C. The nonequilibrium Green's function method for transport

Transport is studied by means of the nonequilibrium Green's function (NEGF) method. In the following, we discuss the physical meaning of the necessary equations. A detailed introduction and derivations can be found in [21–25].

The Green's function of the system is defined as

$$G(E) = (E - H'_k)^{-1}, \quad (4)$$

where the *effective Hamiltonian*

$$H'_k = H_k + \Sigma_{\text{in}} + \Sigma_{\text{out}} \quad (5)$$

is composed of the Hamiltonian  $H_k$  of the closed quantum system (1) and the self-energies  $\Sigma_{\text{in}}$  and  $\Sigma_{\text{out}}$  (defined below). A Fourier transform from the energy to the time domain shows that the matrix elements of the Green's function  $G_{i,j}(t)$  describe the response of the state  $j$  at time  $t$  after a  $\delta(t)$ -excitation of the state  $i$  at time  $t = 0$  [21, 22]. Hence, the Green's function describes the propagation of excitation through the many-body states of the quantum system.

The self-energy matrix elements,

$$\begin{aligned} \Sigma_{\text{in}r,s} &= -i\eta \delta_{r,\text{in}} \delta_{r,s}, \\ \Sigma_{\text{out}r,s} &= -i\eta \delta_{r,\text{out}} \delta_{r,s}, \end{aligned} \quad (6)$$

indicate the ingoing and outgoing states, where the excitation enters and leaves the system from the environment, see Figure 2. The transport is studied between these two states. For the self-energies we have used the so called wide-band approximation [26], where the density of states of the environment is constant ( $\sim \eta$ ) for all considered energies. This is certainly not a microscopic exact model of the environment, but it captures the essential effect: The self-energies are a non-Hermitian modification of the Hamiltonian, so in general its eigenvalues are complex. The imaginary part of the eigenvalues indicates the finite lifetime or energy-broadening of the states due to the coupling to the environment. The broadening is parametrized by  $\eta$  for which we will take in the following  $\eta = 1$ .

The self-energies  $\Sigma_{\text{in}}$  and  $\Sigma_{\text{out}}$  can break the centrosymmetry of the system. We shall consider only self-energies under which the system Hamiltonian  $H_k$  and the effective Hamiltonian  $H'_k$  are centrosymmetric. In the following, we chose as the ingoing state  $|1\rangle = |1, 1, \dots, 1, 0, \dots, 0\rangle$ , where all the fermions are shifted to the left. As the outgoing state we take  $|N\rangle = |0, 0, \dots, 0, 1, \dots, 1\rangle$ , where all the fermions are shifted to the right. These states are clearly related to each other by centrosymmetry, which in turn implies the centrosymmetry of the effective Hamiltonian if  $H_k$  is centrosymmetric.

The transmission probability between the ingoing and outgoing states is given by

$$T(E) = 4\text{Tr}(\text{Im}(\Sigma_{\text{in}}) G \text{Im}(\Sigma_{\text{out}}) G^\dagger) = |2G_{\text{in,out}}|^2. \quad (7)$$

Note that in the last equality, we have used the fact that the self-energy matrices Eq. (6) have only one non-vanishing matrix element. This equation, which is known also as the Caroli formula [27], has a clear physical interpretation. As the Green's function describes the propagation of excitations in the system, the transmission is just the absolute square of the matrix element of the Green's function, which connects the ingoing and outgoing states.

The total current through the system is given by integrating the transmission over all energies, i.e.

$$I = \int_{-\infty}^{\infty} dE T(E). \quad (8)$$

## III. RESULTS AND DISCUSSION

### A. Ensemble averaged transmission and current distributions

In the following, we illustrate our results for a system consisting of  $l = 6$  single-particle states which are occupied with  $n = 1, 2, \dots, l - 1$  fermions and coupled by  $k$ -body ( $k = 1, 2, \dots, n$ ) interactions. One could argue that interactions between  $k \sim n$  particles are averaged out and not relevant. However, in the case  $k = n$  the Hamiltonian (1) is identical to the Gaussian orthogonal ensemble (GOE) [8], which has minimum information [28]. Moreover, transport in biomolecules takes place

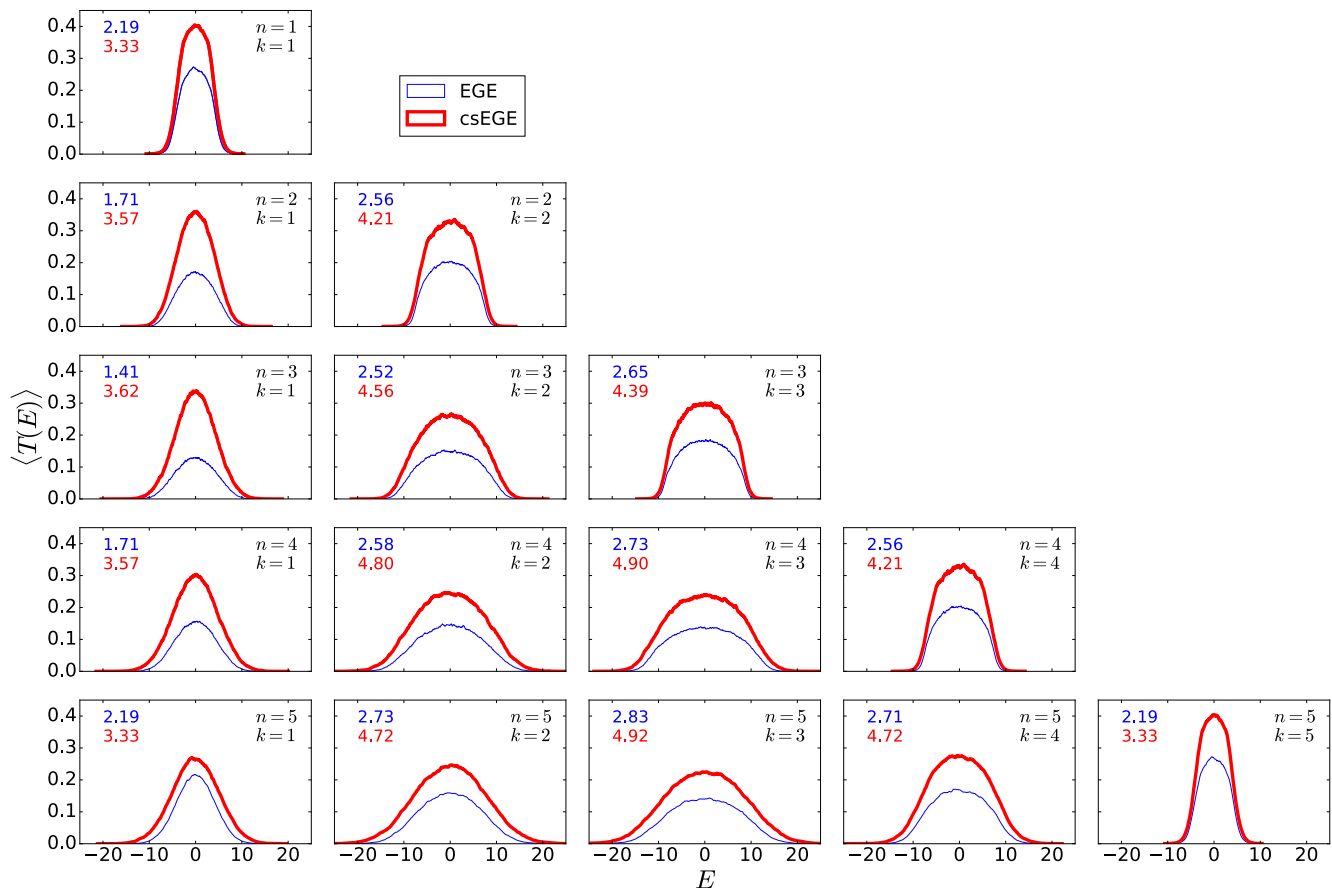


Figure 3. (color online) Ensemble averaged transmission  $\langle T(E) \rangle$  as a function of the energy  $E$  for a system of  $l = 6$  single-particle states. Each column has fixed value of  $k$ , for  $k = 1, 2, \dots, n$ , while each row corresponds to a fixed value of  $n$ , for  $n = 1, 2, \dots, l - 1$ . The ensemble consists of  $10^4$  realizations. The results corresponding to the EGE are displayed by the blue-thin curves, while the red-thick curves illustrate the csEGE results. Imposing centrosymmetry increases considerably the ensemble averaged transmission for all energies.

on a sub-picosecond time-scale [29], where correlations between many particles can be relevant. This justifies to address all rank of interactions. Our results remain valid for other small system sizes, as shown in the Appendix for systems consisting of  $l = 8$  and  $l = 10$  single-particle states. Unless stated otherwise, for each concrete set of parameters, we have calculated an ensemble of  $10^4$  realizations with and without centrosymmetry being imposed.

We have already seen in Figure 1 that centrosymmetry enhances significantly the coherent transmission  $T(E)$  through the system. The ensemble averaged transmission  $\langle T(E) \rangle$  is displayed in Figure 3, where all combinations of  $n$  and  $k$  are shown. We observe that in the case of centrosymmetric embedded Gaussian random matrix ensemble (csEGE) the transmission is for all energies higher than for the non-centrosymmetric Gaussian ensemble (EGE), i.e.  $\langle T_{\text{csEGE}}(E) \rangle > \langle T_{\text{EGE}}(E) \rangle$ . In both cases the spectral span of the transmission, i.e., the width of the conduction band, is maximal for  $k \sim n/2$  and increases with  $n$ . That is, the system is conductive for a wider range of energies. The ensemble averaged trans-

mission is peaked around the center of the conduction band at  $E = 0$ .

In particular, for fixed  $n$  (along a row in Figure 3) maximal values of the transmission are attained at  $k = 1$  and  $k = n$  for the EGE as well as for the csEGE. The shape of the maxima differs in the two cases; for  $k = 1$  the maximum is strongly peaked, whereas for  $k = n$  it is broader and rounded. This behavior can be observed also for larger systems, see the Appendix, though the values for  $k = 1$  are slightly larger than for  $k = n$ . These cases are of interest because transport is typically more efficient in a narrow energy band around  $E = 0$ . This effect is most pronounced for the extrema at  $k = n = 1$  and  $k = n = 5$ .

In Figure 4 we present the frequency histograms  $\mathcal{N}(I)$  of the current, calculated by means of Eq. (8). We observe that the average current  $\langle I \rangle$ , whose values are included in the insets and are illustrated by the vertical lines, is enhanced significantly when centrosymmetry is imposed. This trend is independently from the actual value of the parameters  $(n, k)$ . Moreover, the average current is maximal if the system is almost filled, i.e.

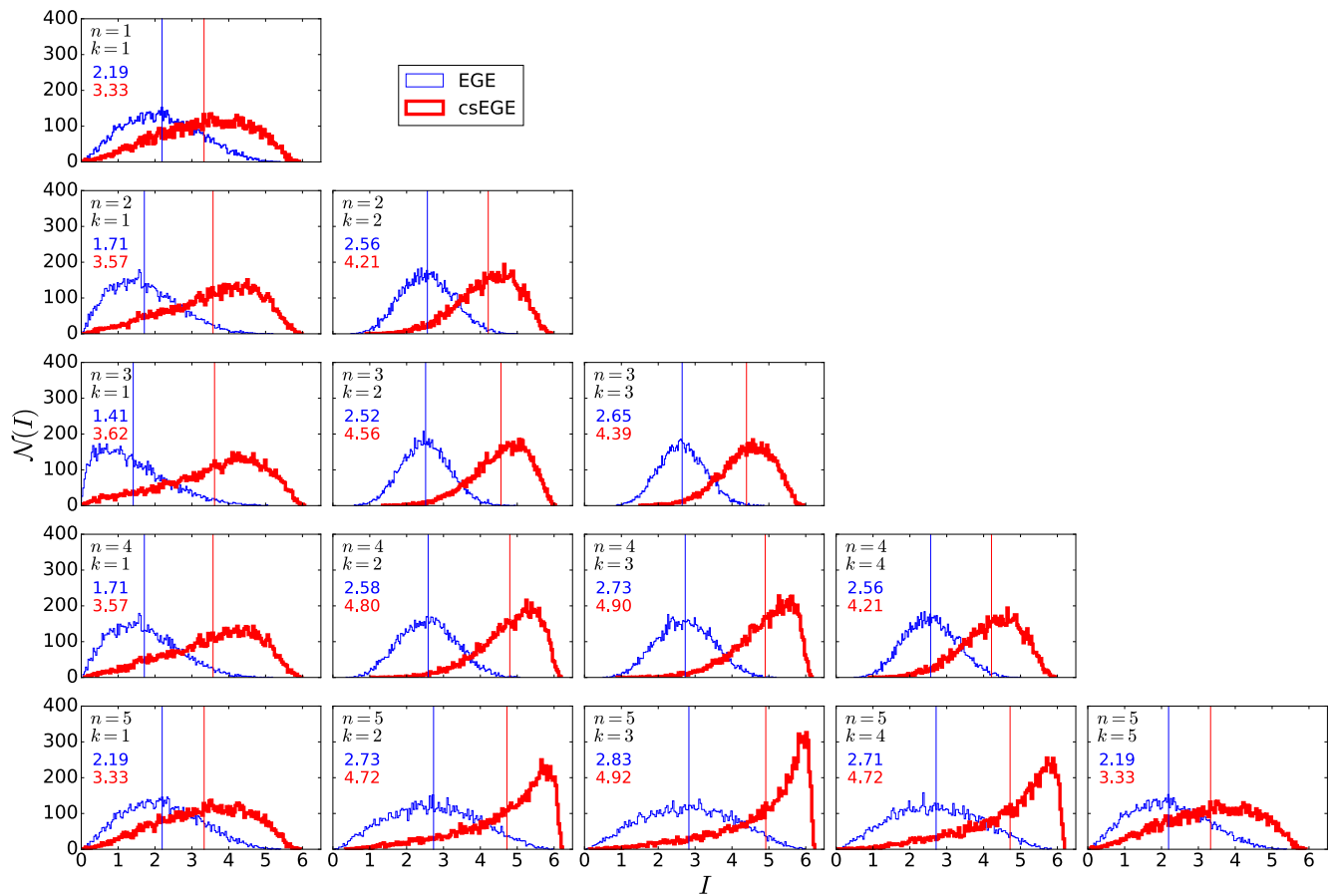


Figure 4. (color online) Frequency histogram of the current for  $10^4$  realizations for the EGE (blue-thin) and the csEGE (red-thick). The arrangement of the figures is the same as in Figure 4. The average current  $\langle I \rangle$  is indicated by the vertical lines and their values are shown in the insets. The current is maximal if the system is almost filled  $n = l - 1$  and the rank of interaction between the particles  $k \sim n/2$ .

$n = l - 1$ , and the rank of interaction is  $k \sim n/2$ . These statements also apply to the mode (i.e. the position of the maximum) of the current distributions. Note that for larger systems (see the Appendix) the average current is maximal for  $n$  close, but not identical, to  $l - 1$ . These results for stationary transport are fully consistent with our previous results [18], where the dynamic propagation of states was addressed. The effects of centrosymmetry are thus present in time-dependent quantities [5, 6, 18] and also in stationary transport properties.

As we consider finite systems of  $l$  states occupied by  $n$  particles, one may look for particle-hole symmetries in the system. The Hamiltonian  $H_k$  may describe  $n$  particles as well as  $l - n$  holes; yet, the embedded ensemble in general do not display that symmetry, see [20]. Briefly, applying the particle-hole transformation to  $H_k$ , the result is a Hamiltonian that consists of the sum of ranks  $0, 1, \dots, k$  in the hole representation, instead of a single term of rank  $k$ . As for  $k = n$  the  $H_k$  are taken from the GOE, we observe particle-hole symmetry in these cases, i.e. results for the parameters  $(n, k = n)$  and  $(l - n, k = l - n)$  are identical. This can be seen clearly in

the ensemble averaged transmission as well as in the frequency histogram of the total current, see Figure 3 and Figure 4 as well as Figure 12 - Figure 15 in the Appendix. Further symmetries can be observed only in the distribution of the total current (Figure 4), where we observe numerically that the cases  $(n, k = 1)$  and  $(l - n, k = 1)$  are identical.

As illustrated in Figure 1, we observe that centrosymmetry yields many resonance peaks with perfect transmission, i.e.  $T = 1$ ; for EGE we may find some perfect transmission resonances, but it is not the typical case. Denoting by  $\epsilon_j$  the eigenvalues of  $H_k$ , these resonances are located at energies  $E \approx \text{Re}(\epsilon_j)$ . This motivates us to study in Figure 5 the statistics of the transmission at these energies  $\text{Re}(\epsilon_j)$  (top row), and compare them with the transmission at random energies (bottom row) for the EGE and the csEGE in the case  $n = l - 1$  and all possible values of  $k$ . These histograms confirm our observation about Figure 1 that centrosymmetry generates many resonances with perfect transmission. Note that perfect transmission is also observed when the transmission is evaluated at random values of the energy (within the

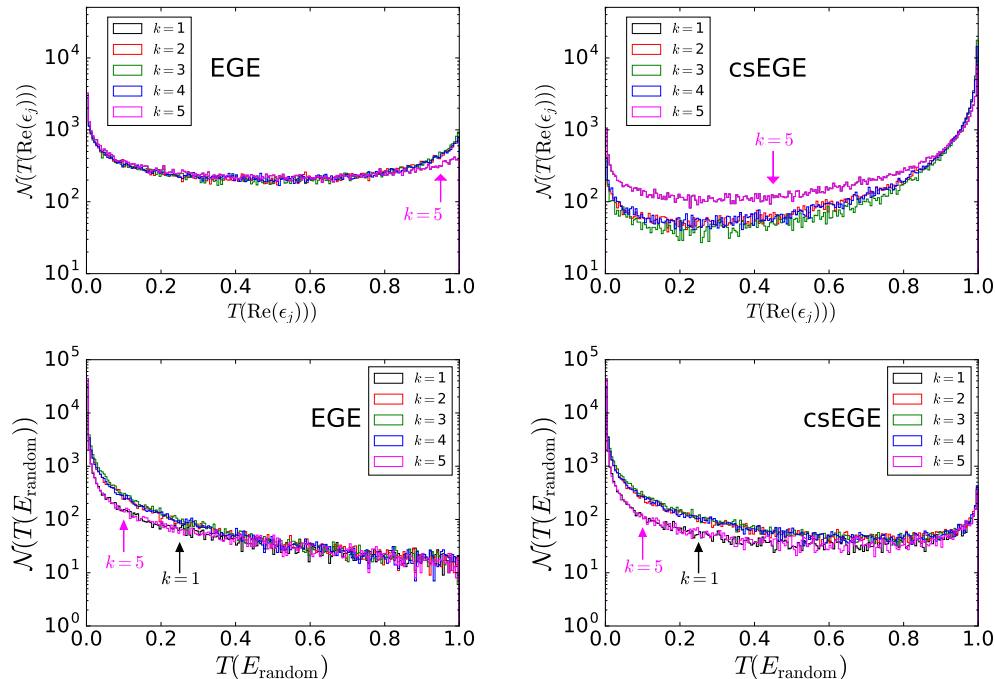


Figure 5. (color online) Top row: Histogram of the transmission evaluated at the real part of the complex eigenenergies of  $H'_k$ , where the resonances are located approximately. The histogram confirms our observation from Figure 1 that centrosymmetry generates many resonances of optimal transmission  $T(\text{Re}(\epsilon_j)) = 1$ . Bottom row: The histogram of the transmission at random energies confirms this property and furthermore, shows the general trend that centrosymmetry enhances the transmission for all energies, see Figure 3. Note that the vertical axes are in logarithmic scale.

conductance band); yet, the relative frequency is higher by about two orders of magnitude for the csEGE. We also note that there is a weak dependence on  $k$ , such that  $k \sim n/2$  dominates for larger values of the transmission. These results show the general trend that centrosymmetry enhances the transmission for all energies, see Figure 3, which implies a higher total current.

In Figure 6 we show the distribution of  $2G_{\text{in,out}}(\text{Re}(\epsilon_j))$  in the complex plane for  $n = l - 1$  and all values of  $k$ . This quantity is of interest since its modulus squared gives the transmission through the system at  $E = \text{Re}(\epsilon_j)$ , see Eq. (7). As the transmission is bounded to values equal or less than 1, the data points are distributed inside the unit circle. Strong correlations between the real and imaginary part are found for both EGE and csEGE. For the EGE (left column), the data points are clustered around the origin, which corresponds to transmission resonances with low conductance. In contrast, in the case of csEGE (right column), the data points display an accumulation on the boundary of the unit circle, around the poles, corresponding to resonances of optimal transmission. We can also see that this accumulation is larger for  $k \sim n/2$ .

## B. Statistics of the spectral decomposition of the transmission

In order to have more insight into the effects induced by centrosymmetry on transport, we use the spectral decomposition of the Green's function. Then, the transmission is expressed as

$$T(E) = |2G_{\text{in,out}}(E)|^2 = \left| \sum_{j=1}^N \frac{\Upsilon_j}{E - \epsilon_j} \right|^2, \quad (9)$$

where

$$\Upsilon_j \equiv 2\phi_{j,\text{in}}\phi_{j,\text{out}}. \quad (10)$$

Here, the  $\phi_{j,\text{in}}$  or  $\phi_{j,\text{out}}$  are the in/out components of the  $j$ th eigenfunction of the effective Hamiltonian  $H'_k$ . Note that  $H'_k$  is non-Hermitian but it has the property  $H'_k{}^\dagger = H'_k{}^*$ . In this case the eigenstates can be chosen in such a way that they fulfill the orthogonality relation  $\langle \phi_i | \phi_j \rangle = \delta_{ij}$  and the completeness relation  $1 = \sum_j |\phi_j\rangle \langle \phi_j|$ , which have been used in Eq. (9).

In the following, we will focus on the case  $n = l - 1 = 5$ , which corresponds to the optimal case in terms of transport; see Figure 3 and Figure 4. Our results hold also for other  $n$ .

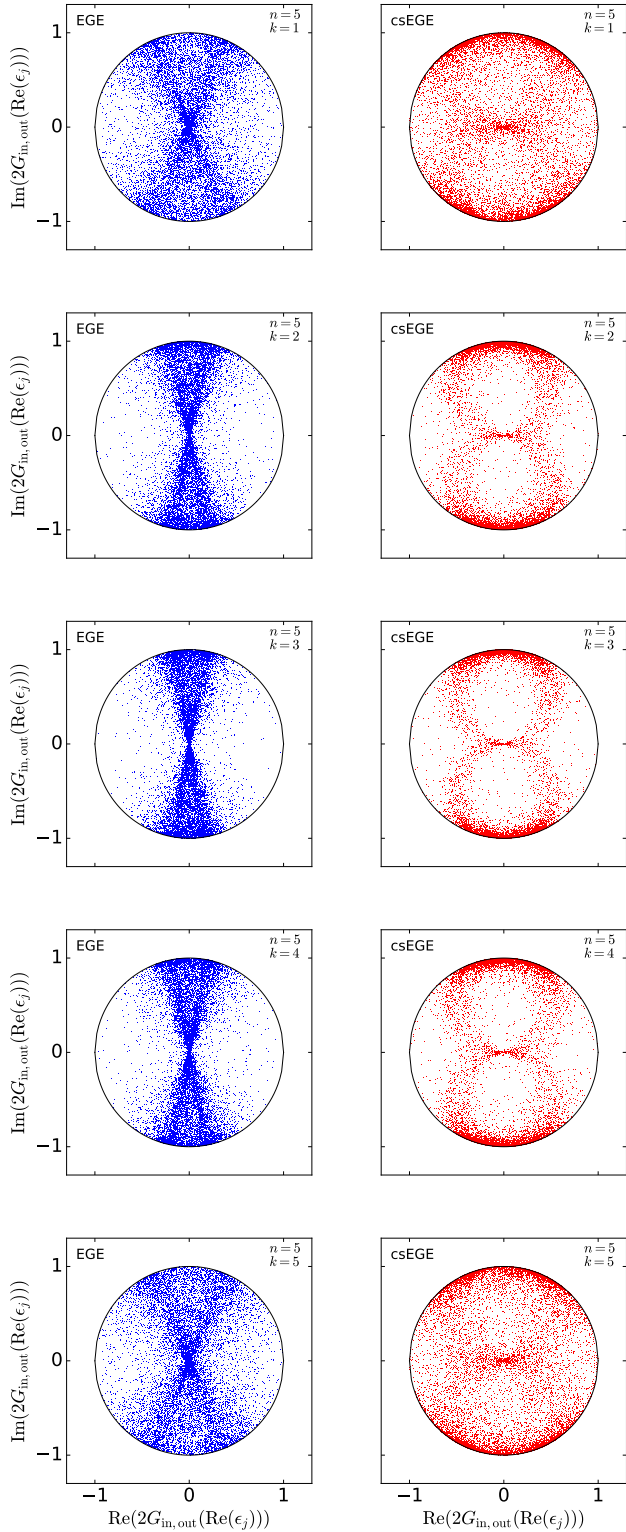


Figure 6. (color online) Distribution of  $2G_{\text{in,out}}(\text{Re}(\epsilon_j))$  in the complex plane for 2000 realizations. Strong correlations between the real and imaginary part are observed in both cases. In the case of EGE (left column), data points are concentrated around the origin, which corresponds to transmission resonances of low conductance. For the csEGE (right column), the data points are accumulated on the poles, which corresponds to perfect transmission.

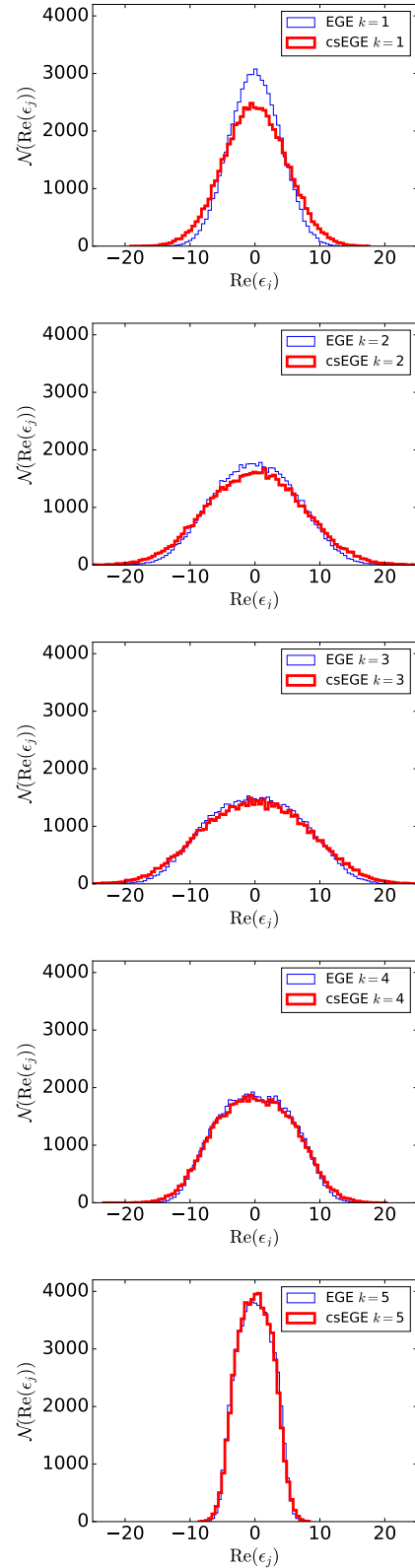


Figure 7. (color online) Histograms of  $\text{Re}(\epsilon_j)$  for  $n = l - 1 = 5$ . The spectral span is maximal for  $k \sim n/2$ , which explains the maximum of the conductance bandwidth at this value, see Figure 3. The csEGE (red-thick histogram) lead to a marginally wider spectral span but the differences decrease for increasing  $k$ .

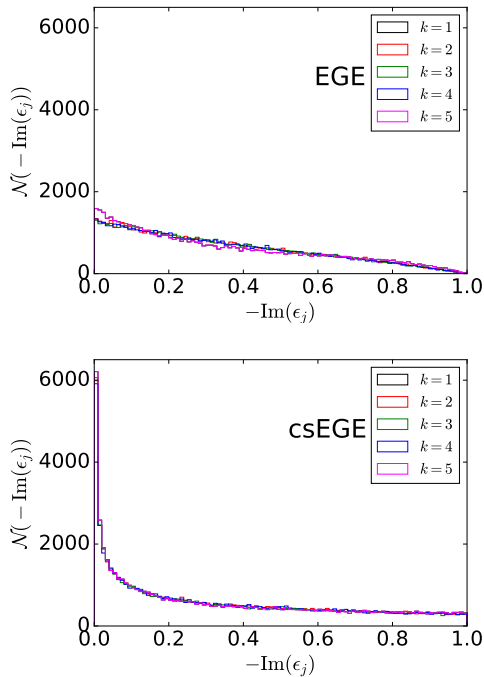


Figure 8. (color online) Distributions of  $\text{Im}(\epsilon_j)$  for  $n = l - 1 = 5$ . The histograms are independent from the rank of interaction  $k$ , displaying a dependence on the presence or absence of centrosymmetry. Centrosymmetry enhances the number of eigenvalues with an imaginary part close to its minimum zero and its maximum  $-\eta = -1$ .

The real part of the complex eigenvalues  $\epsilon_j$  determine the position of the transmission resonances; their distributions in terms of  $k$ , are shown in Figure 7. We observe that centrosymmetry has only weak effects; it increases marginally the spectral span. The differences between the two cases are decreasing when  $k$  increases. In both cases the spectral span is maximal for  $k \sim n/2$ . These observations explain that the width of the conduction band is maximal for  $k \sim n/2$  and that it is marginally wider for the centrosymmetric case.

In turn,  $\text{Im}(\epsilon_j)$  is related to the width of the transmission peaks, see Figure 1. The distributions of  $\text{Im}(\epsilon_j)$  are presented in Figure 8. As shown, their structure is essentially independent of  $k$ . Comparing the EGE and csEGE cases we find that centrosymmetry amplifies the occurrence of the extrema: the number of eigenvalues with  $\text{Im}(\epsilon_j) = 0$  and  $\text{Im}(\epsilon_j) = -\eta = -1$  is larger when centrosymmetry is present. The former value corresponds to resonances of vanishing width, while the latter is related to broad resonances. Then, the histograms for the EGE show that the number of broad resonances vanishes linearly as  $\text{Im}(\epsilon_j) \rightarrow -\eta$ , while for the csEGE this limit attains a constant.

The corresponding distributions  $\Upsilon_j$ , see Eq. (10), is shown in Figure 9. It displays similar properties as the distributions of  $\text{Im}(\epsilon_j)$ . That is, csEGE shows a larger

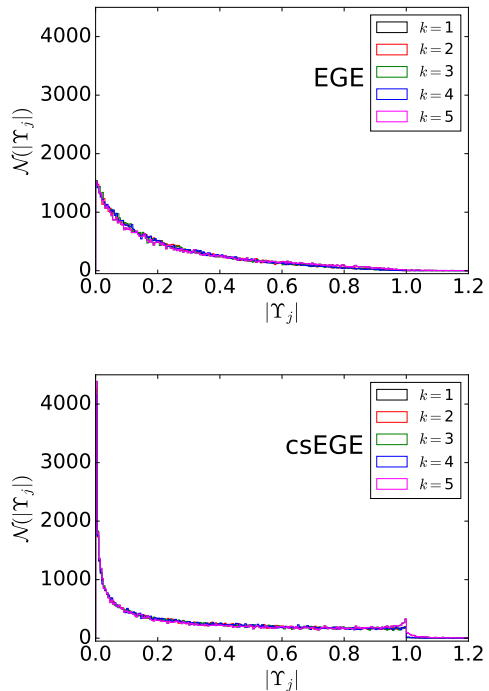


Figure 9. (color online) The histograms of  $|\Upsilon_j|$  have similar properties as the histograms of  $-\text{Im}(\epsilon_j)$  in Figure 8.

frequency of events displaying zero and the maximal values of  $|\Upsilon_j|$  than the EGE, and the distributions are essentially independent from  $k$ . This motivates us to investigate the correlations between  $|\Upsilon_j|$  and  $\text{Im}(\epsilon_j)$ .

In Figure 10, we plot  $|\Upsilon_j|$  versus  $\text{Im}(\epsilon_j)$  illustrating strong correlations among these quantities. While in the EGE case the data points are scattered in the triangular region  $|\Upsilon_j| \lesssim -\text{Im}(\epsilon_j)$ , in the case of the csEGE the data appear on the line  $|\Upsilon_j| \sim -\text{Im}(\epsilon_j)$  or above it.

The histograms of the ratio  $\tau_j \equiv |\Upsilon_j|/\text{Im}(\epsilon_j)$  in Figure 11 show these strong correlations from another perspective. In view of Eq. (9), the quantity  $\tau_j$  yields an estimate of the transmission by taking into account the main resonance only and neglecting all interference effects, i.e. the other terms of the sum. For the EGE the distribution is mainly located between 0 and 1, with peaks at these values, dominated especially by the  $k \sim n/2$  case. In turn, for the csEGE the values of  $\tau_j$  are peaked strongly at 1 with a decaying tail beyond 1 but without any  $\tau_j$  smaller than 1. Note also the difference in the vertical scales. The  $\tau_j$  may attain values larger than 1 because the phases are neglected, which cause the transmission to be equal or less than 1. These two histograms close our statistical analysis to understand how centrosymmetry enhances transport. They confirm that centrosymmetry enhances the extrema and induces strong correlations which generate numerous transmission resonances of perfect transport ( $T = 1$ ), see Figure 5.



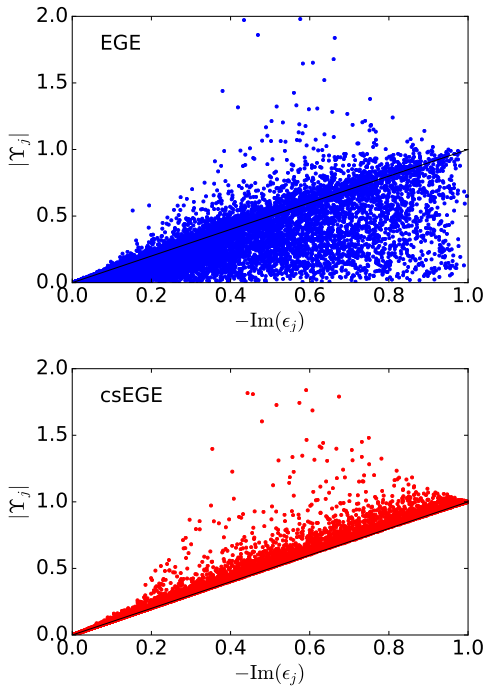


Figure 10. (color online) Distribution of  $|\Upsilon_j|$  versus  $-\text{Im}(\epsilon_j)$  for ensemble of 2000 realizations. Centrosymmetry imposes strong correlations. While in the case of arbitrary EGE the data points are located mainly in a triangle  $|\Upsilon_j| \lesssim -\text{Im}(\epsilon_j)$ , in the case of csEGE the data points are pinned on the line  $|\Upsilon_j| \sim -\text{Im}(\epsilon_j)$  or above it.

#### IV. CONCLUSIONS & OUTLOOK

In this paper, we have analyzed the stationary transport properties of fermions through small disordered interacting networks, which are modeled by embedded Gaussian ensemble of random matrices. We have addressed the influence of centrosymmetry and have shown that the transport is enhanced significantly if centrosymmetry is present. This applies for the transmission  $\langle T(E) \rangle$ , which is a function of the energy of the excitation, as well as for the averaged total current  $\langle I \rangle$  through the system, see Figure 3 and Figure 4, respectively.

We have shown that centrosymmetry induces many transmission resonances of perfect transport (i.e.  $T = 1$ ) which enhances the transport in the overall conduction band, see Figure 1 and Figure 5. We have also seen that—independent from the fact whether the system is centrosymmetric or not—the width of the conduction band is maximal for  $k \sim n/2$  and increases with  $n$  until the system is almost filled. In contrast, for  $k = 1$  and  $k = n$  the conduction band width is minimal. In the best case, which appears when the system is almost filled  $n = l - 1$  and the rank of interaction is  $k \sim n/2$ , centrosymmetry enhances the averaged total current by 75% and its mode increases by a factor of two. For larger systems, see the Appendix, the best cases appear for values of  $n$  close but

less than  $l - 1$ ; the improvement of the transport by centrosymmetry is even stronger. Moreover, we observe that the distribution of the total current for the csEGE has a very large dominating peak for  $n = l - 1$ , close to the highest observed currents. Our results are therefore in perfect agreement with our previous work [18].

Using the spectral decomposition of the Green's function, we have shown that centrosymmetry enhances the extrema, see Figure 8 and Figure 9. The number of resonances with minimal (0) and maximal (1) width (proportional to  $\text{Im}(\epsilon_j)$ ) and weight ( $\propto |\Upsilon_j|$ ) increases. Centrosymmetry also induces strong correlations between the width and the weight of the resonances, see Figure 10 and Figure 11. This suppresses destructive interference effects in the system and thus, causes backscattering-free transmission resonances which enhance the overall transport. We interpret these results as a manifestation that centrosymmetry is an important property for the design of quantum networks with efficient transport characteristics.

Comparing with [5], we find that a doublet-structure in the Hamiltonian is not required to improve the transport in the system. Centrosymmetry, which is imposed at the one particle level and taken to the  $k$  and  $n$  particle space, and the  $k$ -body interaction, are enough to enhance significantly the transport characteristics of the system.

Some degree of decoherence will be inevitably present in biomolecules at room temperature and, to some extent, also in quantum devices. Therefore, we are currently extending the model to study the effects of decoherence on the transport efficiency using the statistical approach which we have developed recently [30–32].

#### ACKNOWLEDGMENTS

We are very grateful to T. Gorin and M. Vyas for useful discussions and helpful remarks. T.S. acknowledges a postdoctoral fellowship from DGAPA-UNAM. Financial support from CONACyT research grant 219993 and PAPIIT-DGAPA-UNAM research grant IG100616 is acknowledged.

#### Appendix: Systems with $l = 8$ and $l = 10$ single-particle states

In this Appendix we show, equivalently to Figure 3 and Figure 4, the ensemble averaged transmission and the frequency histogram of the total current for systems consisting of  $l = 8$  and  $l = 10$  single-particle states. Note that although we have added only up to 4 single-particle states to the system studied in the main text, the dimension of the Hilbert space  $\binom{l}{n}$  is up to 10 times larger. Note also that the spectral span, the width of the conduction band and hence, the total current increase with  $l$ , see [20]. We observe qualitatively the same properties as for the smaller system with  $l = 6$ , except that maximal

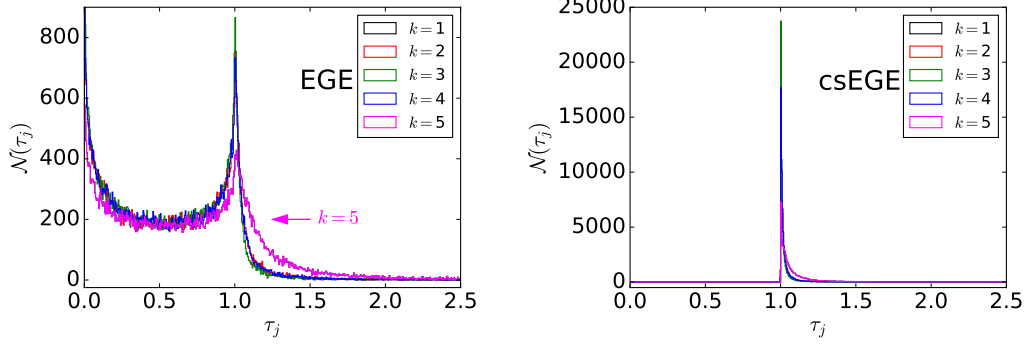


Figure 11. (color online) Histograms of the quotient  $\tau_j \equiv |\Upsilon_j / \text{Im}(\epsilon_j)|$ . For EGE this quotient is distributed mainly between 0 and 1 with maxima at these points. In contrast, for csEGE the distribution of  $\tau_j$  is pinned to 1 without any value less than 1. This indicates the increase of resonances of perfect transmission due to centrosymmetry, see Figure 5.

values of the total current are observed also for fillings close but less than  $l - 1$ . The mode of the distribution of the total current for the csEGE is strongly peaked for

$n = l - 1$ , close to the highest observed currents. The statistics of the spectral decomposition is the same as for the system discussed in the main text.

- 
- [1] R. E. Fenna and B. W. Matthews, *Nature* **258**, 573 (1975).
- [2] S. Bose, *Contemporary Physics* **48**, 13 (2007).
- [3] T. Scholak, F. de Melo, T. Wellens, F. Mintert, and A. Buchleitner, *Phys. Rev. E* **83**, 021912 (2011).
- [4] T. Zech, R. Mulet, T. Wellens, and A. Buchleitner, *New J. Phys.* **16**, 055002 (2014).
- [5] M. Walschaers, J. F.-d.-C. Diaz, R. Mulet, and A. Buchleitner, *Phys. Rev. Lett.* **111**, 180601 (2013).
- [6] M. Walschaers, R. Mulet, T. Wellens, and A. Buchleitner, *Phys. Rev. E* **91**, 042137 (2015).
- [7] T. A. Brody, J. Flores, J. B. French, P. A. Mello, A. Pandey, and S. S. M. Wong, *Rev. Mod. Phys.* **53**, 385 (1981).
- [8] T. Guhr, A. Müller-Groeling, and H. A. Weidenmüller, *Phys. Rep.* **299**, 189 (1998).
- [9] G. M. Nikolopoulos and I. Jex, *Quantum State Transfer and Network Engineering* (Springer, 2014).
- [10] M. B. Plenio, J. Hartley, and J. Eisert, *New J. Phys.* **6**, 36 (2004).
- [11] M. Christandl, N. Datta, A. Ekert, and A. J. Landahl, *Phys. Rev. Lett.* **92**, 187902 (2004).
- [12] M. Christandl, N. Datta, T. C. Dorlas, A. Ekert, A. Kay, and A. J. Landahl, *Phys. Rev. A* **71**, 032312 (2005).
- [13] S. Bose, A. Casaccino, S. Mancini, and S. Severini, *Int. J. Quantum Inf.* **07**, 713 (2009).
- [14] D. Burgarth and S. Bose, *New J. Phys.* **7**, 135 (2005).
- [15] A. Casaccino, S. Lloyd, S. Mancini, and S. Severini, *Int. J. Quantum Inf.* **07**, 1417 (2009).
- [16] L. Benet and H. A. Weidenmüller, *J. Phys. A* **36**, 3569 (2003).
- [17] V. K. B. Kota, *Embedded Random Matrix Ensembles in Quantum Physics* (Springer, 2014).
- [18] A. Ortega, M. Vyas, and L. Benet, *Ann. Phys. (Berlin)* **527**, 748 (2015).
- [19] A. Cantoni and P. Butler, *Linear Algebra and its Applications* **13**, 275 (1976).
- [20] L. Benet, T. Rupp, and H. A. Weidenmüller, *Ann. Phys. (N.Y.)* **292**, 67 (2001).
- [21] S. Datta, *Electronic Transport in Mesoscopic Systems* (Cambridge University Press, 1997).
- [22] S. Datta, *Quantum Transport: Atom to Transistor* (Cambridge University Press, 2005).
- [23] E. N. Economou, *Green's Functions in Quantum Physics* (Springer, 2006).
- [24] M. Di Ventra, *Electrical Transport in Nanoscale Systems* (Cambridge University Press, 2008).
- [25] J. C. Cuevas and E. Scheer, *Molecular Electronics: An Introduction to Theory and Experiment* (World Scientific, 2010).
- [26] C. J. O. Verzijl, J. S. Seldenthuis, and J. M. Thijssen, *J. Chem. Phys.* **138**, 094102 (2013).
- [27] C. Caroli, R. Combescot, P. Nozieres, and D. Saint-James, *J. Phys. C: Solid State Phys.* **4**, 916 (1971).
- [28] R. Balian, *Il Nuovo Cimento B* **57**, 183 (1968).
- [29] G. R. Fleming, S. F. Huelga, and M. B. Plenio, *New J. Phys.* **13**, 115002 (2011).
- [30] T. Stegmann, M. Zilly, O. Ujsághy, and D. E. Wolf, *Eur. Phys. J. B* **85**, 264 (2012).
- [31] T. Stegmann, O. Ujsághy, and D. E. Wolf, *Eur. Phys. J. B* **87**, 30 (2014).
- [32] T. Stegmann, *Quantum transport in nanostructures: From the effects of decoherence on localization to magnetotransport in two-dimensional electron systems*, Ph.D. thesis, University Duisburg-Essen (2014).

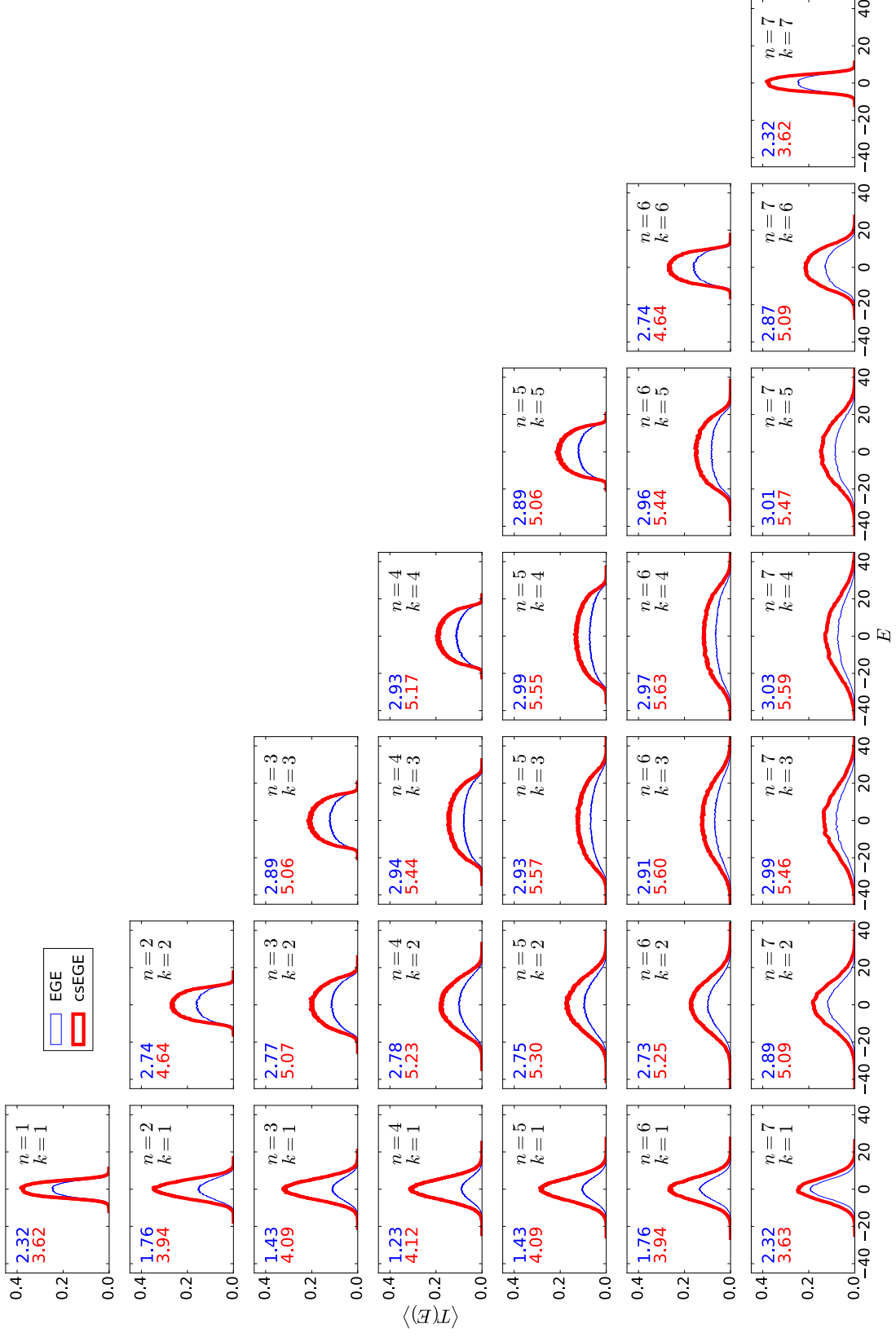


Figure 12. (color online) Ensemble averaged transmission  $\langle T(E) \rangle$  for a system with  $l = 8$  single-particle states. The arrangement of the figures is the same as in Figure 3.



Figure 13. (color online) Frequency histogram of the current for a system with  $l = 8$ . The arrangement of the figures is the same as in Figure 4.

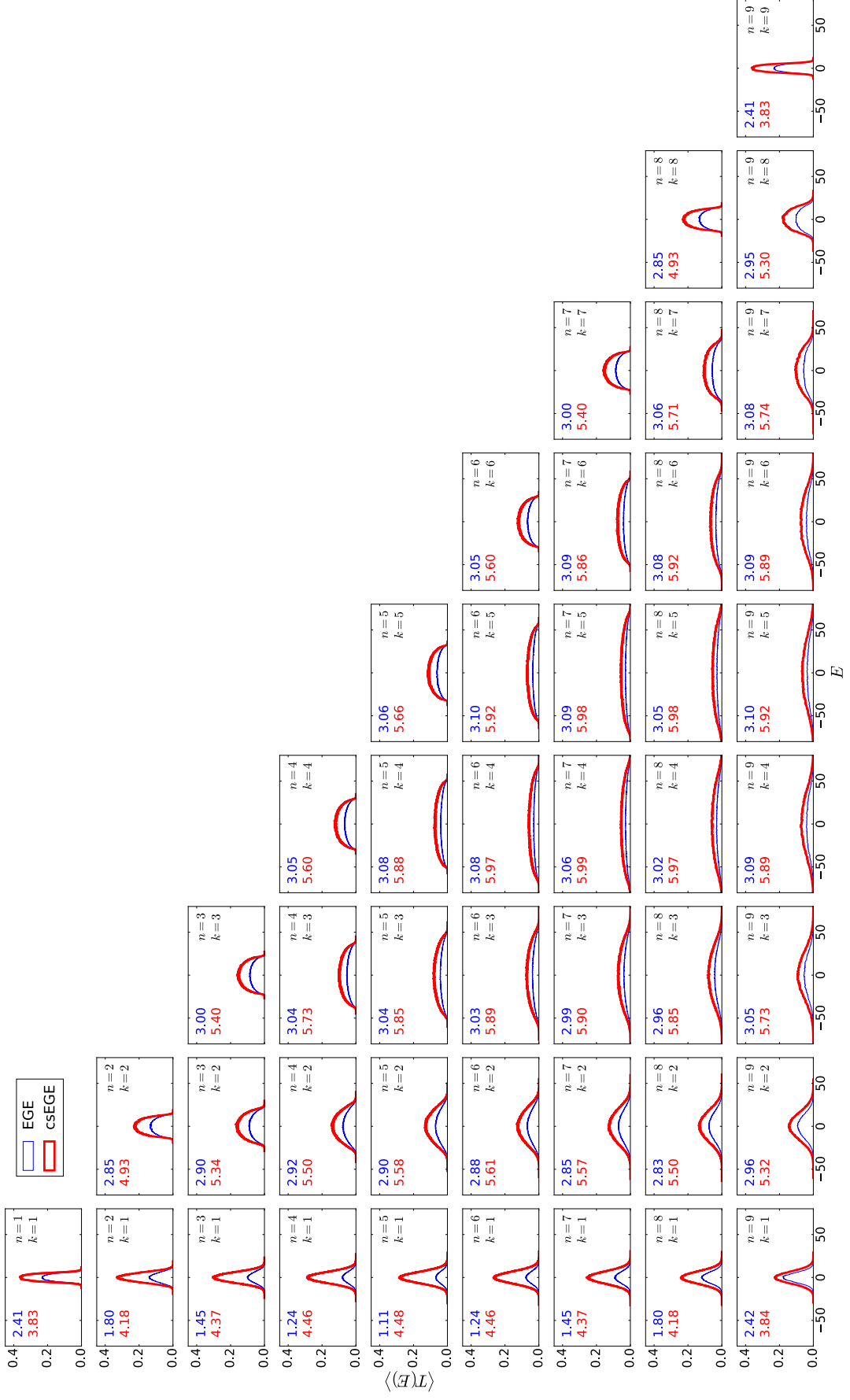


Figure 14. (color online) Ensemble averaged transmission  $\langle T(E) \rangle$  for a system with  $l = 10$ . The arrangement of the figures is the same as in Figure 3.

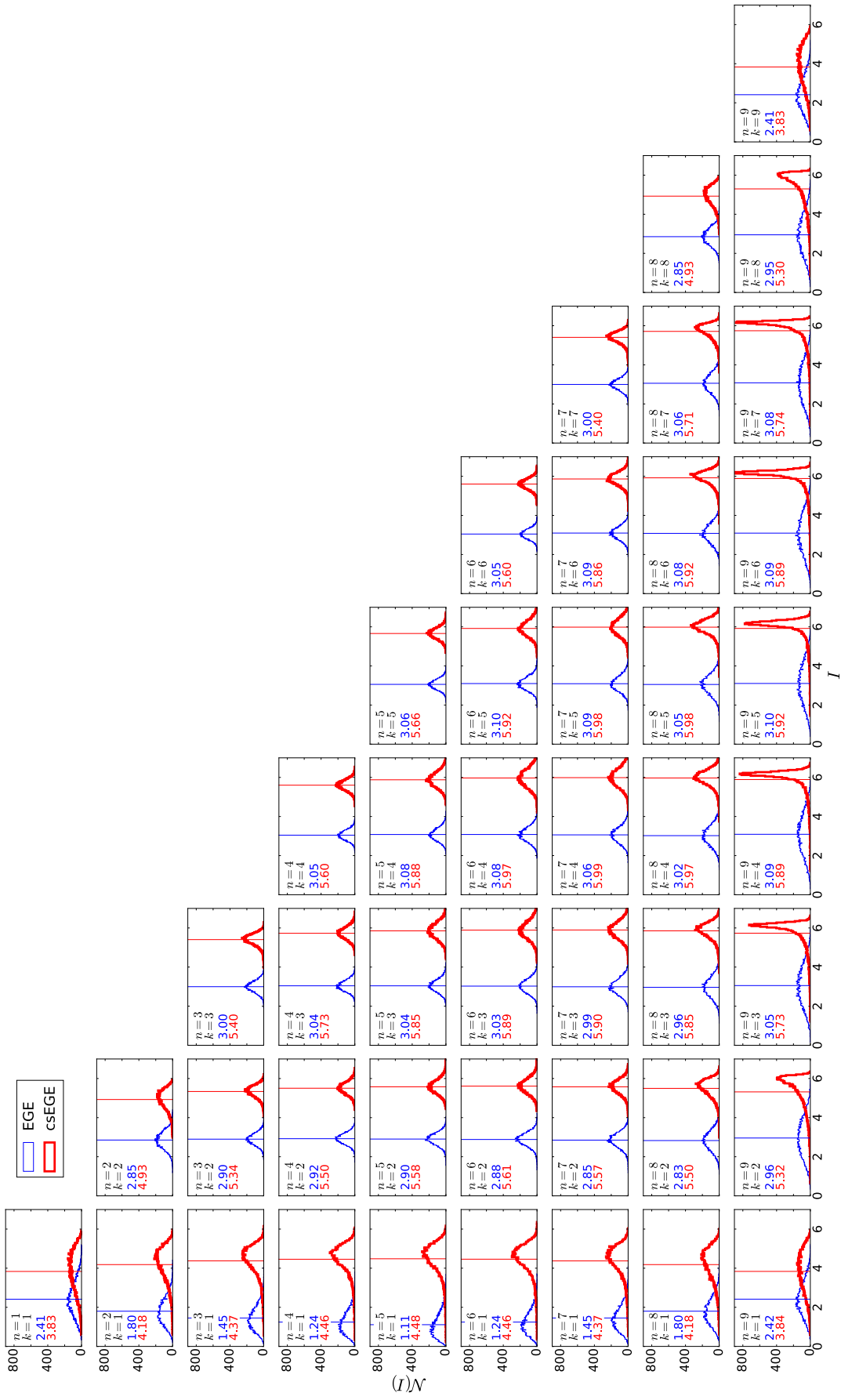


Figure 15. (color online) Frequency histogram of the current for a system with  $l = 10$ . The arrangement of the figures is the same as in Figure 4.